

Measuring fiber position errors from spectral data

Jian-Jun Chen^{1,2,3}, Zhong-Rui Bai^{1,2,3}, A-Li Luo^{1,2} and Yong-Heng Zhao^{1,2}

¹ National Astronomical Observatories, Chinese Academy of Sciences, Beijing 100012, China;
jjchen@nao.cas.cn

² Key Laboratory of Optical Astronomy, National Astronomical Observatories, Chinese Academy of Sciences, Beijing 100012, China

³ University of Chinese Academy of Sciences, Beijing 100049, China

Received 2014 March 6; accepted 2014 May 16

Abstract Precise fiber positioning is crucial to a wide field, multi-fiber spectroscopic survey such as the Guoshoujing Telescope (the Large Sky Area Multi-Object Fiber Spectroscopic Telescope, LAMOST). Nowadays, most position error measurements are based on CCD photographic and image processing techniques. These methods only work for measuring errors orthogonal to the telescope optical axis, but there are also errors that lie parallel to the optical axis of the telescope, such as defocusing, and errors caused by the existing deviation angle between the optical axes of a fiber and the telescope. Directly measuring the two latter types of position errors is difficult for an individual fiber, especially during observations. Possible sources of fiber position errors are discussed in brief for LAMOST. By constructing a model of magnitude loss due to the fiber position error for a point source, we propose an indirect method to calculate both the total and systematic position errors for each individual fiber from spectral data. Restrictions and applications of this method are also discussed.

Key words: techniques: multi-fiber — fiber spectroscopy — spectrophotometry

1 INTRODUCTION

The Guoshoujing Telescope (also called the Large Sky Area Multi-Object Fiber Spectroscopic Telescope, LAMOST) is a specially designed reflecting Schmidt telescope with 4000 fiber units mounted on a focal plane with a 5° field of view (FOV). Fibers in LAMOST feed light from targets into 16 spectrographs (Cui et al. 2012). The Two-degree-Field (2dF) Galaxy Redshift Survey and Sloan Digital Sky Survey (SDSS) have achieved great successes in the last two decades. LAMOST is also conducting a major multi-fiber spectroscopic survey (Zhao et al. 2012), and releasing spectra of more than one million targets each year.

Large spectroscopic surveys primarily require the signal-to-noise ratio (SNR) of observed spectra to reach certain criteria, and the SNR strongly depends on the proportion of light feeding the effective aperture of each fiber from the target. Considering that the size of each LAMOST fiber is only 0.32 mm in diameter (corresponding to $3.3''$), in terms of engineering, it is not easy to reach the position accuracy of about $1''$ for 4000 fiber units, and even harder to maintain them during the entire cycle of operation during a survey over a year. Thus, routinely measuring the fiber position

errors and retaining the position accuracy are crucial for reaching the SNR requirements for a survey like LAMOST. Moreover, besides the random position errors, the spatial distribution of fiber position errors in the focal plane may display a systematic pattern across fields that are repeatedly observed over a period of time. This could lead to position dependent selection effects and eventually jeopardize certain scientific goals of the survey.

There are many sources of fiber position errors. Newman (2002) gave a detailed discussion of the sources that impact the fiber position accuracy, especially in the cases of SDSS and 2dF. There are three types of position errors according to Newman (2002): position errors orthogonal to the optical axis of the telescope, errors parallel to the optical axis and telecentric alignment errors, which arise from an angle that exists between the optical axes of the telescope and fibers. Although LAMOST does not adopt the magnetic puck-position system of 2dF or the drilled-plate system of SDSS, Newman's discussion is still suitable for LAMOST in general. Moreover, because LAMOST employs 4000 double revolving fiber position units on the focal plane to move the fibers synchronously (Xing et al. 1998; Cui et al. 2012), there are some new sources of error that could affect the positioning accuracy, e.g. a malfunction in the stepping motors, errors in machining and installation of the motors and fiber units, etc.

Due to the importance of fiber position accuracy and having a diversity of sources in determining position errors, many efforts have been made to measure and then correct the position errors. So far, most such efforts in measurements are based on CCD photographic and image processing techniques. LAMOST routinely takes photographic measurements to calibrate the focal surface coordinates and check the working condition of fiber units. In practice, measurement of LAMOST fiber positioning is conducted about every three months in order to test the precision of the fiber positioning system. A series of CCD images is taken and processed to analyze the focal plane, while the fiber-heads are illuminated from the end of spectrographs and arranged in multiple testing positions to calibrate the focal plane coordinates with the help of a standard spot array (Cui et al. 2012). Through this process, malfunctioning fiber units can then be identified and replaced.

Recently, a number of modified CCD photographic methods have been proposed, either to achieve higher precision (Gu et al. 2012), or to cut down the time required for measurement in order to have the capability for near real-time measurement and feedback during the observation (Wang et al. 2012). However, all the methods based on photography are only able to measure the position errors orthogonal to the optical axis, which offer little help in dealing with errors parallel to the optical axis and the error arising from fiber telecentric alignment.

In this paper, a new approach is proposed to measure the total position errors, including orthogonal, parallel and telecentric alignment errors. This approach is based on a model describing the magnitude loss of a point source due to position errors in various seeing conditions. Because the light from a point source and the light from the sky background are both directed into a fiber's aperture, in principle the magnitude of sky brightness can be calculated by providing the magnitude of a point source from an input catalog, and measurements of the target and sky flux can be made from the observed spectrum. Actually, the sky brightness calculated from this method varies with the value of position errors, i.e. the greater the position error is, the larger the sky brightness becomes. Of course this is not entirely true because the flux corresponding to the magnitude from the input catalog is not completely directed into the fiber aperture due to position errors. Given a true sky brightness magnitude, the difference between the true and calculated sky brightnesses represents the magnitude loss due to fiber position errors. The values of position error can then be solved using the previously mentioned model.

In the rest of this paper, Section 2 briefly explores the sources of fiber positioning errors, particularly in the case of the LAMOST fiber positioning system. Section 3 introduces the concept of equivalent position error. It only has an orthogonal component that is nonzero, and has magnitude loss that is caused by all three types of positioning errors. Then a model is presented to quantitatively describe the correlation between the magnitude loss of a point source and the equivalent

position error. Section 4 describes a procedure that determines the value of equivalent position error by comparing the true sky brightness with the sky brightness calculated from the input catalog and spectral flux. In Section 5, several aspects of this measurement are discussed, including the influence of atmospheric transmittance, possible sources of error in this method, and a comparison of SNR and photographic measurements.

2 SOURCES OF POSITION ERRORS FOR LAMOST

Newman (2002) gave a comprehensive description of the sources that cause a mismatch between the positions of fibers and the resulting image in spectroscopic telescopes that use multiple fiber systems, particularly in the cases of SDSS and 2dF. LAMOST incorporates an efficient fiber positioning system. It is able to reconfigure fibers in minutes with its ability to adjust 4000 fibers simultaneously. The spherical focal surface is actually composed of the head-ends of 4000 individual fiber units. In addition to the sources of position errors listed in Newman (2002), the precision of fiber positioning in LAMOST strongly depends on the accuracy of fabrication and installation for these 4000 fiber units. Maintaining an accurate positioning system depends on the working conditions of these fiber units.

Table 1 gives a summary of the sources of position errors and the corresponding measurement/correction when dealing with position errors that are applied during the operation of LAMOST.

Table 1 Sources of Position Errors and Measurement / Correction Applied to LAMOST

Sources of Position Errors	Measurement / Correction Applied to LAMOST
Errors orthogonal to the optical axis	
Astrometry	Input catalog and guiding system
Aberration, parallax and proper motion	Input catalog and guiding system
Conversion to focal surface coordinates	Calibration CCD and ‘fiber scan’ (Cui et al. 2012)
Fiber and fiber unit mounting	Calibration CCD images
Temporal variation in image scale	Guiding CCD images and active optics
Collimation and field rotation	Guiding CCD images and active optics
Atmospheric distortion and guiding	Guiding CCD images / guiding system
Atmospheric differential refraction	Restricted observation area (Donnelly et al. 1989)
Telescope pointing	Guiding system
Stepper motor malfunction	Motor controller feedback and software implementation
Errors parallel to the optical axis	
Shape of focal surface	Manufacturing / installation accuracy of fiber units
Focus errors during observation	Guiding CCD images / adaptive optics
Telecentric alignment error	
Angle between fiber axis and optical axis of telescope	Installation accuracy of fiber units

3 MODEL OF MAGNITUDE LOSS DUE TO POSITION ERRORS

For a point source, the fiber-to-image position mismatch certainly causes flux loss for this target, and thus the resulting spectrophotometric magnitude loss. Conversely, the magnitude loss also leads to measurement of the total position errors in the targeting of a fiber for a point source. Since the total position errors include orthogonal, parallel and telecentric alignment errors, the concept of equivalent position error is introduced in this paper for constructing a model of the decrease in magnitude. The equivalent position error is defined as setting the parallel and telecentric alignment components to zero, and only having a nonzero orthogonal component leftover. This approach causes the effects of magnitude loss to be equivalent to that caused by total position errors.

The image profile of a point source on the focal surface is quite complex, because it has been convolved with the point spread function (PSF) of the telescope, the turbulence of the atmosphere and random motion of guiding adjustment, which are all integrated over the exposure time. In this

paper, the image profile of a point source is adequately modeled by a normalized two dimensional Gaussian (Brodie et al. 1988) with known $\sigma = W/(2\sqrt{\ln 4})$

$$f(x, y) = \frac{1}{2\pi\sigma^2} e^{-\frac{(x-\Delta x)^2 + y^2}{2\sigma^2}}, \quad (1)$$

where Δx is the equivalent position error.

The width of the PSF, W , is measured by the FWHM of point sources which are stars on the guiding CCD images. It is affected by both dome and atmospheric seeing, and any systematic defocusing across the focal plane. In this paper, a constant seeing disk across the focal plane is assumed. Because four guiding CCD cameras are mounted in a square on the LAMOST focal plane (Cui et al. 2012), it is easy to verify if this assumption is satisfied by checking the variation in values of W among images from the four guiding CCDs.

Considering that the diameter of the fiber is $3.3''$, given Δx and W , the flux $F(\Delta x)$ falling into the fiber aperture is computed by the integration

$$F(\Delta x) = \int_{-1.65}^{1.65} \int_{-\sqrt{1.65^2 - x^2}}^{\sqrt{1.65^2 - x^2}} f(x, y) dx dy. \quad (2)$$

Given $\Delta x_0 = 0$ and a set of $\Delta x_i > 0$, the corresponding magnitude loss m_a is

$$m_a(i) = \text{mag}(\Delta x_i) - \text{mag}(\Delta x_0) = -2.5 \log \frac{F(\Delta x_i)}{F(\Delta x_0)}, \quad (3)$$

where $F(\Delta x_0) = F(\Delta x = 0)$ is the flux into the fiber aperture when the equivalent position error is $\Delta x = 0$.

Figure 1 shows the data points from a point source's magnitude loss $m_a(i)$ corresponding to the equivalent position error Δx_i , and the polynomial fitted curves during various seeing conditions (as measured by W).

4 SKY BRIGHTNESS AND EQUIVALENT POSITION ERROR

The flux feeding into the aperture of the i th fiber is actually composed of two components: the flux from the targeted object and the flux from the sky background. These two components fall into exactly the same aperture and are both convolved with the total system response of the telescope and instruments. The sky background is a mixture of airglow, background light from faint celestial objects, zodiacal light, ground pollution light, etc (Roach 1964, Gustafson et al. 2007). A portion is from outside the atmosphere, similar to the light from the targets, but some is not. Therefore, the magnitude of sky brightness m_{sky} can be calculated from the equation

$$m_{\text{obs}}(i) - m_{\text{sky}}(i) = -2.5 \log \frac{\text{flux}_{\text{obs}}(i)}{\text{flux}_{\text{sky}}(i)} + \Delta m_{\text{atm}}(i), \quad (4)$$

where $\text{flux}_{\text{obs}}(i)$ is the flux of a point source targeted by the i th fiber after the sky background has been subtracted; $\text{flux}_{\text{sky}}(i)$ is the flux of sky background light feeding into the i th fiber, which in practice is composed of spectra from nearby sky sampling fibers; $m_{\text{obs}}(i)$ and $m_{\text{sky}}(i)$ are their corresponding magnitudes; and $\Delta m_{\text{atm}}(i) = -2.5 \log(\Delta \text{flux}_{\text{obs, atm}}(i) / \Delta \text{flux}_{\text{sky, atm}}(i))$ represents the difference in magnitude caused by differing thicknesses of the atmosphere through which light from the target and sky background passes.

For each target, the LAMOST input catalog provides the photometric magnitude m_{obj} retrieved from high precision multi-band photometric catalogs, such as SDSS, PanStarrs, the Xuyi Antigalactic Center photometric survey, etc (Zhao et al. 2012). Considering the size of the seeing

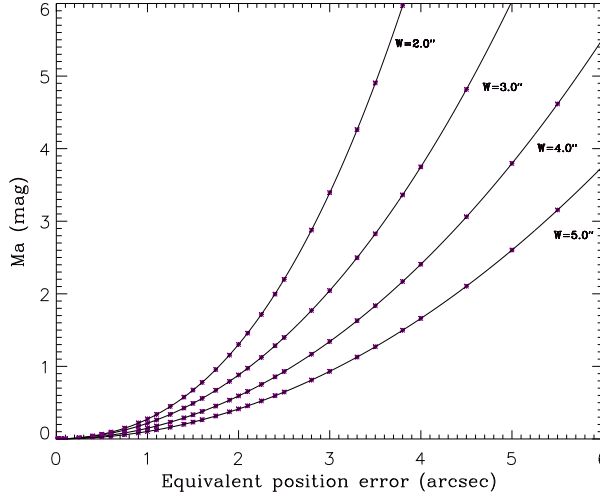


Fig. 1 The model of magnitude loss (m_a) due to the equivalent position error (Δx) for a point source. The various seeing conditions (W) give different polynomial fitting curves.

disks, only part of the target's light falls into the fiber aperture which is $3.3''$ diameter; the corresponding magnitude m'_{obj} is not equal to m_{obj}

$$\begin{aligned}
 m_{\text{obj}} &= m'_{\text{obj}} - 2.5 \log \frac{\int \int_{-\infty}^{\infty} f(x, y) dx dy}{\int \int_{\sqrt{x^2 + y^2} < 1.65} f(x, y) dx dy} \\
 &= m'_{\text{obj}} - 2.5 \log(1/F(\Delta x_0)). \quad (5)
 \end{aligned}$$

For a long time, the night sky, especially the dark night sky, has been regarded as a uniform source for flat field exposures when observations are being acquired. The uniformity of the dark sky at zenith is nearly perfect during a clear, dark night. The relative gradient slowly degrades to one percent per degree to a zenith angle of about 50° , and degrades further to about 2% per degree until the zenith angle is close to 70° (Chromey & Hasselbacher 1996).

Therefore, the differential in sky magnitude among the fibers in one exposure would be very small if this exposure is taken on a clear, dark night, and the zenith angle is limited to within 50° . Under these conditions, the gradient of magnitude for sky brightness among the 4000 fibers across the 5° FOV is less than 0.05 mag. This number is negligible compared to the value we are most interested in, magnitude loss, plotted in Figure 1, where the equivalent position error is larger than $1.0''$.

The value of m_{atm} depends on air mass (Donnelly et al. 1989). Near the zenith angle of 30° , the difference in air mass across a 5° FOV is about 5%, corresponding to a maximal difference of 0.05 mag among 4000 fibers. When zenith angle increases to 50° , the differential in air mass changes to about 10% across 5° , corresponding to a maximum of about 0.1 mag among 4000 fibers. Therefore, there is a need to consider the differential in m_{atm} when the zenith angle is larger than 30° . If we select an exposure such that the pointing of the zenith angle is less than 30° , ignoring the differential in m_{sky} and in m_{atm} among fibers in the 5° FOV, we have

$$m_{\text{sky}}(i) = m_{\text{sky}}$$

and

$$\Delta m_{\text{atm}}(i) = m_{\text{obs,atm}}(i) - m_{\text{sky,atm}}(i) = \Delta m_{\text{atm}}.$$

Note that here $m_{\text{obs}} = m'_{\text{obj}} + m_a$ by definition and let the pseudo sky brightness be $m_{\text{sky}}' = m_{\text{sky}} - \Delta m_{\text{atm}}$; Equation (4) can then be rewritten as

$$\begin{aligned} I(i) &= m'_{\text{sky}} - m_a(i) \\ &= m_{\text{obj}}(i) + 2.5 \log \left\{ \frac{\text{flux}_{\text{obs}}(i)}{\text{flux}_{\text{sky}}(i)} \cdot \frac{1}{F(\Delta x_0)} \right\}, \end{aligned} \quad (6)$$

where $I(i) = m'_{\text{sky}} - m_a(i)$ is defined as the implied sky brightness.

Both items m'_{sky} and $m_a(i)$ in Equation (6) are unknown, but $I(i)$ is calculated from the right-hand side of Equation (6). A histogram of $I(i)$ is plotted in Figure 2. Considering the many random position errors and the large number of fibers targeting point sources in selected exposures (> 3000 for some exposures), it is reasonable to assume that at least some fibers have m_a close to zero, that is, the part on this histogram corresponding to the faintest values. We are able to estimate the sky brightness m_{sky}' on the histogram in Figure 2. Then it is easy to determine the corresponding $m_a(i) = m_{\text{sky}}' - I(i)$ for each individual fiber, and to solve the value of equivalent position error from the model described in Section 3.

Figure 3 shows the equivalent position error distribution of fibers for one exposure, calculated from three specified sky brightness values: the peak, the maximum (with outliers being manually rejected, which is discussed in Section 5.3), and the value at the 3σ cut, where σ is the standard deviation of the half-Gaussian distribution on the right-hand side of Figure 2. The equivalent position error distribution from the peak sky brightness implies the fiber positioning units are working correctly, and ignores the systematic errors that are mainly contributed during guiding motion and defocusing of the whole focal plane. It represents the position errors caused by orthogonal mismatching, the random shifts from defocusing in the focal plane, and the tilt (telecentric alignment error) of individual fibers. The result from the 3σ cut is close to that from the maximum, and it is convenient to exclude the outliers from the implied sky brightness distribution. The shift between the left distribution, calculated from the peak sky brightness, and the other two, $0.5'' \sim 0.7''$ in Figure 3, can be regarded as the value of systematic position error from the guiding motion and defocusing of the whole focal surface.

Figure 4 gives plots of the distributions of implied sky brightness and equivalent position errors on the focal plane. At least for this exposure, there is no conspicuous evidence for a gradient across the focal plane.

5 DISCUSSION

5.1 Width of the PSF, W

As mentioned before, the width of the PSF, W , is given by measuring the FWHM of point sources which are stars on images taken by the guiding CCD. A constant W is assumed across the focal plane. This assumption can be checked by measuring the variation in W among images from four guiding cameras, which are mounted in a square on the focal plane.

In this technique, variation in W is regarded as arising from defocusing, both individually and systematically, so the effects of variation in W contribute to equivalent position error if it is caused by individual fiber defocusing, or tilt and defocusing of the focal plane plate. However, the result could be misleading if it is caused by a local thermal disturbance on the focal plane.

Increasing the value of W will flatten the distribution of equivalent position errors and expand the range of the distribution to the side with larger errors.

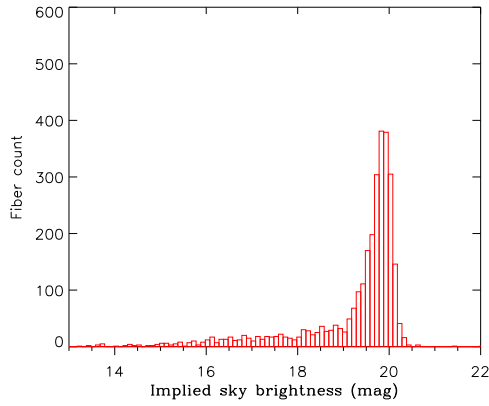


Fig. 2 Histogram representing implied sky brightness $I(i) = m_{\text{sky}}' - m_a(i)$ of one exposure with a seeing disk W of $2.6''$. The peak of the distribution is 19.85 mag. The uniform sky brightness is estimated to be 20.5 mag (at maximum) or 20.38 mag (by using a 3σ cut) on this plot, where σ is the standard deviation on the right side of the peak.

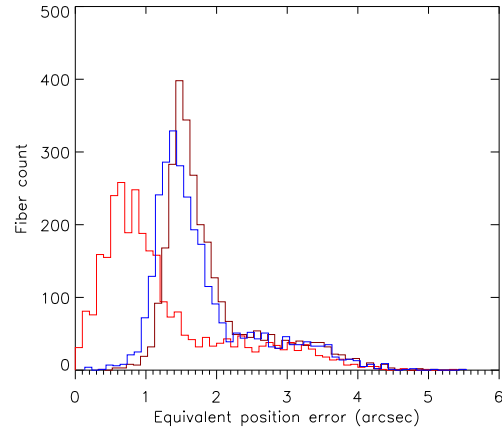


Fig. 3 The distribution of equivalent position errors is solved with the error model in Section 3, while the magnitude loss $m_a(i)$ is from Equation (6) using the sky brightness on Fig. 2. From left to right, three equivalent error distributions are respectively calculated from the sky brightness of the peak, the 3σ cut and the maximum.

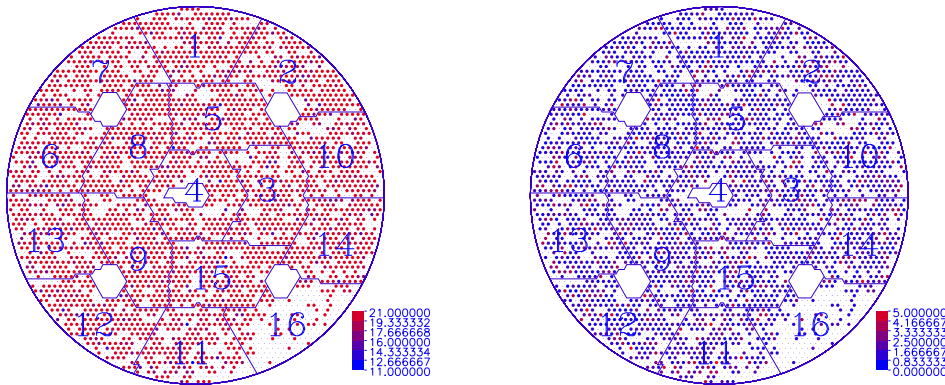


Fig. 4 The implied sky brightness distribution on the focal plane (*left*), and the equivalent position error distribution on the focal plane (*right*). The blank fiber units were not assigned to point targets.

Another notable aspect of W is the guiding motion. According to Newman (2002), we considered the effect on the flux loss due to the integration of guiding motion to be a part of the position errors in this paper and to be a main contributor to the systematic position errors. From another perspective, this effect can also be considered as an extended seeing disk during the exposure. The stacked guiding images could be used to measure this extended W .

5.2 Influence of Atmospheric Transmittance

Since not all components of sky light are from outside the Earth's atmosphere, the integrated atmospheric thickness through which the sky light passes is always less than that through which the target light passes. Therefore, Δm_{atm} also depends on atmospheric thickness. The value of Δm_{atm} is hard to measure in practice, because either the intensity of night sky components or the atmospheric transmittance continually varies during the exposure. We can regard $m_{\text{sky}}(i)$ and $\Delta m_{\text{atm}}(i)$ in Equation (4) as a single quantity, defined as $m_{\text{sky}}'(i)$, because only the uniformity of both is required for Equation (6) to be valid.

The major components of sky light include airglow, aurora and light pollution (Gustafson et al. 2007). The aurora is weak at Xinglong, which has a latitude of about 40° N. Both aurora and airglow are from the top level of the atmosphere at an altitude of about 100 km or higher, so they have a similar effective atmospheric thickness as lights from targets. Therefore, the major contributor to Δm_{atm} is artificial light pollution from the ground. Ice crystals and water droplets in clouds attenuate the light from outside the atmosphere and reflect pollution from the ground (Burke et al. 2010), thus affecting the uniformity of m_{sky} and Δm_{atm} .

5.3 Sources of Measurement Error

Uniformity of both sky brightness and atmospheric transmittance is essential for this method to measure the fiber position error, so a telescope pointing for a selected exposure is limited to an angle close to zenith, e.g. a zenith angle less than 30° . Clear, cloudless exposure conditions are needed. Having a moonless condition is not necessary but the telescope pointing needs to maintain some distance from the Moon in order to avoid the brightness gradient caused by the Moon. For an exposure with a larger zenith angle, $> 50^\circ$, the error caused by the gradient in m_a could be larger than 0.1 mag. It mainly affects fibers with an equivalent position error less than $1.5''$ for good seeing conditions (W) in Figure 1. For fibers having larger equivalent position errors, the final results are not sensitive to this gradient, at least for exposures with small seeing disks.

Stray lights, undetected cosmic rays and an unmasked warm column on CCD images contaminate the target spectrum and lead to the calculated sky brightness being unusually faint. Actually, a few fibers satisfy this kind of situation in the bottom right corner of Figure 2, which have an isolated sky brightness $m_{\text{sky}}' - m_a(i)$ value of about 22. These fibers are rejected when deciding where to cut off the right edge of the histogram.

The assumption that at least some of the fibers with the faintest sky brightness satisfy $m_a(i) = 0$ may not be true. If so, the histogram in Figure 3 would shift leftwards. However, the profile of the distribution of equivalent position errors changes little, and the order of fibers sorted by the value of position error remains unchanged. The precision of data reduction affects the measurement accuracy, especially the precision of sky subtraction.

5.4 Comparison to the SNR and CCD Photographic Methods in Measuring Position Error

Position errors greatly affect the SNR of the observed spectra. Practically speaking, the SNR of a spectrum is often used as an indicator of fiber position errors. Newman (2002) acknowledges that the real-time evaluation of spectral SNR is a tool to compensate for variation in position errors. SNR is also used for statistically selecting the fiber units with large errors. Besides position errors, SNR is also affected by many other factors, such as vignetting, variation in efficiency among spectrographs and CCD cameras, variation in throughput among fibers, etc. Measurement of equivalent position errors overcomes these aspects, because, as a reference, the sky light goes through exactly the same aperture as light from the target, and is convolved with the telescope and instrument response in the same way. From Figure 3, this method implies there is a separation of systematic and random errors.

Equivalent position error measurement and photographic measurement are complementary. The former measures the total position error, but is unable to distinguish the error sources. Photographic measurement could help to estimate the source by providing an orthogonal component of the error, which benefits troubleshooting and provides a solution to locate the bad fiber units.

This equivalent position error method is a measurement that is independent of the instrument. It could be easily applied to spectral data of other multi-fiber telescopes to measure the total position errors for individual fibers.

Acknowledgements The authors would like to thank Prof. Hu Jingyao and Prof. Wang Gang for their helpful discussions. We are grateful to the anonymous referee for valuable comments and suggestions. The Guoshoujing Telescope (the Large Sky Area Multi-Object Fiber Spectroscopic Telescope, LAMOST) is a National Major Scientific Project built by the Chinese Academy of Sciences. Funding for the project has been provided by the National Development and Reform Commission. LAMOST is operated and managed by the National Astronomical Observatories, Chinese Academy of Sciences.

References

- Brodie, J. P., Lampton, M., & Bowyer, S. 1988, *AJ*, 96, 2005
- Burke, D. L., Axelrod, T., Blondin, S., et al. 2010, *ApJ*, 720, 811
- Chromey, F. R., & Hasselbacher, D. A. 1996, *PASP*, 108, 944
- Cui, X.-Q., Zhao, Y.-H., Chu, Y.-Q., et al. 2012, *RAA (Research in Astronomy and Astrophysics)*, 12, 1197
- Donnelly, R. H., Brodie, J. P., Bixler, J. V., & Hailey, C. J. 1989, *PASP*, 101, 1046
- Gu, Y., Jin, Y., & Zhai, C. 2012, in *Society of Photo-Optical Instrumentation Engineers (SPIE) Conference Series*, ed. R. Navarro, 8450, 84503E, 9
- Gustafson, B. Å. S., Witt, A. N., Dwek, E., et al. 2007, *Transactions of the International Astronomical Union, Series A*, ed. O. Engvold (Cambridge: Cambridge University Press), 26, 161
- Newman, P. R. 2002, *PASP*, 114, 918
- Roach, F. E. 1964, *Space Sci. Rev.*, 3, 512
- Wang, M., Zhao, Y., & Luo, A. 2012, in *Society of Photo-Optical Instrumentation Engineers (SPIE) Conference Series*, ed. R. Navarro, 8450, 84503D, 10
- Xing, X., Zhai, C., Du, H., et al. 1998, in *Advanced Technology Optical/IR Telescopes VI*, *Society of Photo-Optical Instrumentation Engineers (SPIE) Conference Series*, ed. L. M. Stepp, 3352, 839
- Zhao, G., Zhao, Y.-H., Chu, Y.-Q., Jing, Y.-P., & Deng, L.-C. 2012, *RAA (Research in Astronomy and Astrophysics)*, 12, 723